Mechanical Systems and Signal Processing 168 (2022) 108640

Contents lists available at ScienceDirect

Mechanical Systems and Signal Processing

journal homepage: www.elsevier.com/locate/ymssp

Image-based operational modal analysis and damage detection validated in an instrumented small-scale steel frame structure

Cecilia Rinaldi [a,*], Jacopo Ciambella [b], Vincenzo Gattulli [b]

[a] DICEAA, University of L'Aquila, via G. Gronchi 18, 67100, L'Aquila, Italy
[b] DISG, Sapienza – University of Rome, via Eudossiana 18, 00184, Rome, Italy

ARTICLE INFO

Communicated by J. Slavič

Keywords:
Structural health monitoring
Digital image correlation
High-speed camera
Time domain
Frequency domain
Damage detection

ABSTRACT

The use of image-based techniques in structural dynamics is constantly growing thanks to the decrease in the cost of high-speed cameras and the improvement in image processing algorithms. Compared to traditional sensors, such as accelerometers or velocimeters, the use of fast cameras for data acquisition allows the number of measurements points to be significantly increased. However, such an abundance of points, not always lead to an increased accuracy of damage detection algorithms. With this in mind, we compare different damage detection techniques by using displacement data and modal quantities. A small scale steel frame structure is used to validate the damage detection by using measurements acquired through a high-speed camera with different image processing techniques. The Hybrid Lagrangian Particle Tracking (HLPT) algorithm and Digital Image Correlation (DIC) are both used to extract displacement measurements from images. The results are compared with those obtained with seismic class accelerometers which are normally used in the lab for such an application. Damage localization and intensity have been determined through image-based measurements without losing the accuracy obtained with accelerometers.

1. Introduction

In the field of Structural Health Monitoring (SHM), vision-based techniques have emerged as suitable alternative to traditional sensors as they allow multiple points and contactless measurements [1]. They are non-invasive techniques and do not have the burden of modifying the dynamics of the structure by adding mass or rigidity to it.

Latest advances in the field are summarized in [2] where the experience gained from the development of the vision-based sensors for structural dynamic response measurement and SHM are describe with examples of structural identification, structural model updating, damage detection, and cable force estimation. The paper [3] provides an overview of recent applications of computer vision techniques in the field to civil infrastructures by distinguishing inspections and monitoring. A review of computer vision-based structural health monitoring at local and global levels is carried out in [4]. Local level analysis includes applications to detect defects, such as cracks, spalling, delamination, rust, and bolt loosening, while global analysis includes displacement measurement, vibration serviceability, modal identification, model updating, damage detection, cable force monitoring, load factor estimation, and structural identification using input–output information. A discussion about the latest applications of vision-based vibration monitoring of structures and infrastructures is provided in [5] by giving specific attention to full-scale field tests.

The operating principle of every image based dynamic technique is the comparison of images taken at different times. The number of frames per second that can be recorded is a compromise with the sensor accuracy: lower sensor resolutions allow higher frame

* Corresponding author.
E-mail address: cecilia.rinaldi@graduate.univaq.it (C. Rinaldi).

https://doi.org/10.1016/j.ymssp.2021.108640
Received 8 May 2021; Received in revised form 7 November 2021; Accepted 9 November 2021
Available online 5 December 2021

rates, thus higher detectable frequencies but reduce the spatial resolution of the measurements, thus the capability of detecting low amplitude vibrations. On the other hand, high resolution sensors can be used to detect motion of a large scale structure, but with frequency limited to few frames per second. Currently available commercial cameras allow the capturing of images of the order of 10 megapixel at frequencies of up to 1000 Hz [6].

In terms of hardware, an extensive review of the camera models suitable for SHM was carried out in [4]. Camera models are classified in portable, USB web and industrial. A portable camera (e.g. 1920 × 1080 pixels, 60 fps) can provide high resolution, be equipped with zoom lens and can be suitably used for close-range measurements. The USB web cameras provide high resolution, low frame rate and they are generally used for close-range measurement since the measurement distance is limited by the use of embedded lenses. They have fixed resolution and frame rate or multiple resolution-frame-rate modes (e.g. 1920 × 1080 pixels, 30 fps; 1080 × 720 pixels, 30 fps). Among the others, industrial cameras can provide the highest frame rates as well as resolution, including real-time displacement monitoring and image acquisition for post-processing, they are programmable, controlled by computer and can use additional lenses for image acquisition. For industrial cameras only the maximum frame rate is provided as a reference (e.g. 2048 × 1536 pixels, 120 fps), but the actual frame rate can be defined by the user. Adjustable region of interest and subsampling features allow lower-resolution output formats at much higher frame rates. In [7], for instance, a high-speed camera with full resolution of 1920 × 1440 pixels and a frame rate of 500 fps was used to record the in-plane dynamic behaviours of a two-story frame structure and, as described in [8], a camera with a maximum resolution of 1024 × 1024 pixels at 6400 fps was used and adjusted at 384 × 384 pixels at 36000 fps (36 kHz) to capture ultrasonic guided waves generated in a polyethylene plate.

In terms of algorithms, different techniques can be applied to extract the dynamic feature of interest, these include: point tracking, edge tracking techniques and image blurring.

One of the first attempt to use recorded images to detect the dynamic movement of a structure was proposed in [9]. At that time, the hardware capabilities were limited to 25 fps but spline interpolation was used to improve the resolution of the measurements, assuming a continuous and smooth character of the dynamic effect.

A point tracking algorithm based on the detection of distinct features was used in [10] for structural identification; the advantage of this approach was to not requiring markers on structure. In that work, the corner detection method suggested by Harris and Stephens [11] was applied to extract the features, whereas the Kanade–Lucas–Tomasi (KLT) algorithm [12] allowed the tracking.

In [7] the location of damage in steel frames was conducted using a 500 fps camera. First, they determined the best marker positions and shapes for image processing algorithm, then the response of the intact and damaged structure to forced vibrations was recorded and analysed with a damage detection algorithm based on modes shape differences. In [13] the problem of inserting markers on the structure was partially solved by using a colour laser. Testing were carried out on a beam-like structure in which target for the image processing algorithm were applied through a laser on both the damaged and the undamaged structure. The damage detection algorithm was based on the modal curvature shape extracted from the frequency response function with a peak-peaking algorithm.

Although the use of markers on the structure can significantly improve the results of the image processing, there are many practical situations in which insertion of markers to the structure could be an issue. In these cases, edge detection algorithms can be used [6,14,15], yet they require high image resolutions, high-contrast, thus they are especially suited for slender structures. In [16], the edge detection algorithm was applied to evaluate the dynamics of an entire cable in a bridge structure, an effort that would have not been feasible by covering the entire cable with markers. A method for detecting the edge of the cable based on the wavelet transform on the images was presented in [17], they eventually detect the location of the cable failure, and compared the results in terms of natural frequencies of the cable extracted by the image processing method and the laser measurement. The edge detection method was utilized to record vibrations of a simple two-arc beam for obtaining the dynamic characteristics of the healthy and damaged structure in [18].

As for the research carried out by McCarthy et al. [19], Image de-blurring technique was used to monitor small scale laboratory models as well as large scale test. Such a technique partially alleviate the inherent compromise that exists when selecting sensors for monitoring of dynamic structures. Instead of capturing vibrations using very high speed imaging, a high-resolution long-exposure photograph is used, in which the localized object image becomes motion blurred. A specialized image registration algorithm would be necessary to make measurements from such a motion blurred image [20,21].

All the image-based algorithms have the disadvantage of requiring a high level of expertise to process the acquire data with a long processing time compared to traditional sensors for which the data is often available real-time and onsite. For such a reason a proper comparison of the different image processing techniques should take into account the processing time as an additional figure of merit.

The Digital Image Correlation (DIC) and Hybrid Lagrangian Particle Tracking (HLPT) algorithms are applied in this paper to image data recorded during an experimental campaign conducted on a 4-dofs small-scale steel frame structure. In addition, seismic class acclerometers are used as a reference for the dynamic measurements. Data from image analysis are processed with the usual Operational Modal Analysis (OMA) techniques and the results of the analysis used in a damage detection problem. To evaluate the performance of the different damage localization algorithms several damage scenarios were simulated numerically before conducting the experimental campaign. On the real structure, the damage is introduced by removing the two steel bracing located on the third floor of the frame.

The organization of the paper is as follows: Section 2 describes the two image processing algorithms used in this work; Section 3 summarizes the damage identification techniques applied to numerical and experimental campaigns; in Section 4 a sensitivity analysis in terms of damage intensity and position is carried out, whereas the results of the experimental campaign are illustrated in Section 5, which also contains the main results of the image analysis. Section 6 is devoted to comments and conclusions.

2. Visual tracking algorithms

A classification of different visual tracking algorithms along with the feature tracked is reported in [4]. In this section, the focus is on the two techniques mostly used in the literature, the image correlation technique and the feature tracking method, to whose categories the algorithms used in this work belong, i.e. DIC technique [22] and HLPT algorithm [23].

The *correlation-based template matching* (applied in [24]) is based on a template, a selected Region Of Interest (ROI), which slides across another image to search the best matching. Two algorithms are usually applied to evaluate the similarity between template and overlapped regions of the image for ROI matching: the sum of squared differences and the cross-correlation methods. DIC follows a similar approaches. Unlike the template matching, DIC first divides the whole image into multiple sub-regions with grids and uses template matching to calculate the displacement of the sub-region; whilst, the displacement in the whole image is obtained by interpolation. Usually, in dynamic testing only some preassigned markers are tracked with DIC rather than all pixels to reduce the computation time.

The *full field dense optical flow* method is used in [25] allows the evaluation of the optical flow between two images by assuming brightness constancy and temporal regularity. Optical flow is the velocity estimation of a video and it is a vector pointing from the initial position to the end location of the selected pixel. The method based on *sparse optical flow* first extracts the feature points from the images and then calculate the optical flow. The feature points are a subset of the given images (e.g. a sub-image with 5×5 pixels) with distinct features (i.e. intensities, gradients in different directions, textures) [26].

2.1. Digital Image Correlation

The DIC technique used in this paper is the version implemented in the GOM Correlate software (www.gom.com). The algorithm is able to track areas where reference markers have been assigned or where a random distribution of features is present. In this work, this latter approach was used by distributing over the structure sand particles. The random distribution of the particles guarantees that each subset can be clearly identified and distinguished from its neighbourhood.

2.2. Hybrid Lagrangian Particle Tracking algorithm

The HLPT algorithm is based on the solution of the optical flow equation and selects areas of each image where the higher brilliance gradients exist. These areas can be associated to feature points to be tracked from frame to frame. The HLPT algorithm consists of two steps: particle detection and temporal tracking. The detection of a particle in a high-medium-density image prescribes the solution of the optical flow equation which have two unknown velocity components associated to a single pixel. Therefore, the equation is computed in a window centred at the pixel location and the solution, i.e., the displacement vector of the interrogation window between two consecutive frames, is determined through a least square optimization. A set of positions, associated with the displacement vector predictor, which makes the optimization problem well-posed, is detected. Those positions are defined as features and are associated to the centroid coordinates. The set of validated particle image locations and the displacement vector predictor associated to the particle, obtained through the approximated solution of the optical flow equation, are finally used as input data for the tracking algorithm. To identify successive positions of the same particle and extract its displacement, the nearest neighbour principle is employed (in particular that with the minimum Eulerian distance from the position determined with the displacement predictor). This method differs from the 'classical' nearest neighbour one thanks to the use of the displacement vector predictor which allows it not to be erroneously influenced by fast moving particles with respect to the mean inter-particle distance. For such a reason, HLPT algorithms are often used in particle hydro-dynamics. The work [23] presents an application in fluid mechanics of the particle tracking algorithm. The experimental study provides a description of the fluid kinematics establishing in a wavy bottomed photobioreactor. The image analysis technique Feature Tracking was used to reconstruct the trajectories of tracer particles seeding the fluid under investigation and to determine the velocity field evolution with time.

3. Damage location techniques

In our work, the methods used to identify damage position are classified in two main categories: dynamic response-based and modal-based techniques. The former deals with the analysis of the dynamic response of the structure in the time domain, either through displacements or accelerations, and allows the real time assessment of structural conditions; the latter is based on the identification of modal properties (frequencies and mode shapes) in the frequency domain.

3.1. Techniques based on the dynamic response in the time domain

There are practical situations, such as seismic events, in which the real-time detection of structural modification is of paramount importance. Therefore, time-based identification methods have been investigated by several researchers [27,28] as they do not require prolonged acquisition time. These techniques measure the response (displacements, accelerations or strains) under excitation in order to identify structural damages. When using displacements, for instance, an effective damage index is the so-called inter-storey drift, i.e. the relative displacement between two adjacent floors. In [29] such an index was effectively used to estimate the overall damage of a building during earthquake-like induced vibrations. The inter-storey drift can be evaluated following three

approaches: the maximum of the relative displacement between floors, the relative displacement attained when the maximum deflection at the top floor occurs, and the total maximum storey drift at each level considering all time-steps [30].

In the present paper, all three approaches were evaluated but since the second gave the most accurate results is the one described in the following. Let $t_{\max}$ the time instant at which the maximum displacement at the top floor occurs. At each point i, the inter-storey drift d_i is evaluated by:

$$d_i = u_i - u_{i-1} \quad \text{for} \quad i = 2, \dots, N \quad \text{and} \quad d_1 = u_1 \tag{1}$$

where u_i is the displacement at point i (the deflection of the structure) at $t = t_{\max}$ and N the number of equally spaced measurement points. The damage is located at those indices i at which the Drift Variation (DV) overcome a certain threshold:

$$\mathrm{DV}(i) = \frac{d_i^d - d_i^u}{d_i^u} > \mathrm{DV}^{\mathrm{thr}} \tag{2}$$

where d_i^u and d_i^d are the inter-storey drift of the undamaged and damaged structure respectively.

After evaluating the curvature of the deflection profile of the structure, the Curvature Variation (CV) can be used as an additional damage index. As such, we have defined:

$$\mathrm{CV}(i) = \frac{\chi_i^d - \chi_i^u}{\chi_i^u}, \quad i = 1, \dots, N \tag{3}$$

as the difference between the second derivative of the deflection for the undamaged χ_i^u and damaged χ_i^d specimen. Also in this case, the damage is located at those indices i at which the $\mathrm{CV}(i) > \mathrm{CV}^{\mathrm{thr}}$.

3.2. Techniques based on modal properties in the frequency domain

Damage indices based on the use of mode shapes have attracted a great deal of attention since the early eighties. The basic concept is to identify and locate damage by relying on changes, between damaged and undamaged state, of mode shapes or their derivatives.

To this purpose, the RD (Relative Difference) index [31], based on the comparison between the undamaged ϕ_{ij}^u and damaged ϕ_{ij}^d modal shapes is introduced as:

$$\mathrm{RD}(ij) = \frac{\phi_{ij}^u - \phi_{ij}^d}{\phi_{ij}^u}, \qquad i = 1, \dots, N \qquad j = 1, \dots, L \tag{4}$$

where L is the number of modes considered and N the number of measurement points. The damage is identified at those location where RD overcomes a certain threshold. In this formulation, the mode shapes are normalized to unity with respect to the mass matrix ($\boldsymbol{\Phi}^{\mathrm{T}} \boldsymbol{M} \boldsymbol{\Phi} = \boldsymbol{I}$).

Another damage indicator widely used in literature is the COMAC (COordinate Modal Assurance Criteria) [32] defined by:

$$\mathrm{COMAC}(i) = \frac{\left(\sum_{j=1}^{L} |\phi_{ij}^d \, \phi_{ij}^u| \right)^2}{\sum_{j=1}^{L} \left(\phi_{ij}^d \right)^2 \sum_{j=1}^{L} \left(\phi_{ij}^u \right)^2} \tag{5}$$

where again the mode shapes are normalized to mass. Differently from RD, the damage occurs in correspondence of those indices where the COMAC is lower.

The Curvature Variation (CV) evaluated according to Eq. (3) and applied to mode shape profile is another parameter often used in damage detection algorithms [33]. Maximum CV are located in the damage region whereas RD are often spread all over the structure; for this reason CV are often considered a superior damage indicator.

For shear buildings, a specific identification procedure was proposed in [34,35]. This approach makes use of the damage-induced deflections estimated by modal flexibility from ambient vibration measurements. This method consists in three steps. The first one is the evaluation of the modal flexibility $\mathbf{G}_m$ from natural frequencies and mass-normalized mode shapes; the second step consists in the evaluation of the deflection profile under a positive shear inspection load ($\mathbf{u} = \mathbf{G}_m \mathbf{f}$, where $\mathbf{u}$ is the displacement vector corresponding to the positive shear inspection load vector $\mathbf{f} = \{1\}$). The last step is the damage localization using the damage-induced deflections. As showed in [34], the damage-induced deflections occurs at the damaged floor as long as a proper load is applied to the building. The following index Z, based on a statistical approach, is utilized:

$$Z(i) = \frac{d_i^d - \overline{d_i^u}}{\sigma(d_i^u)} \quad \text{for} \quad i = 1, \dots, N \tag{6}$$

where d_i^d is the inter-storey drift of damaged structure, d_i^u is the undamaged inter-storey drift, $\overline{d_i^u}$ and $\sigma(d_i^u)$ are the mean value and the standard deviation of d_i^u. The damage localization is performed using the condition $Z(i) > Z^{\mathrm{thr}}$.

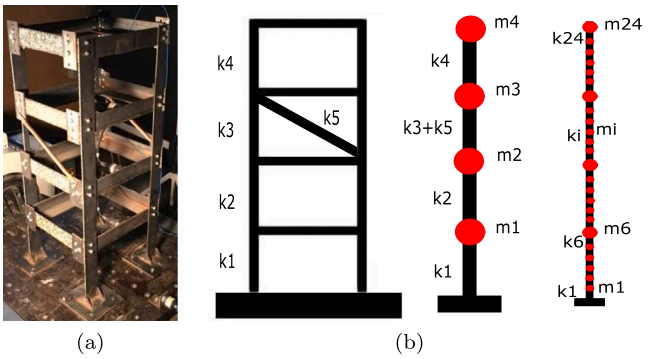

Fig. 1. Shear-type steel frame structure: (a) experimental prototype; (b) numerical model.

4. Numerical case study

In this paragraph, the different damage indices described above are evaluated against a numerical example, to estimate their sensitivity in terms of damage position and intensity. The simulated structure is the same used in the experimental campaign, i.e., a 4-story shear-type steel (S235) structure with two steel bracings in the inter-storey 2–3 (Fig. 1(a)), indicated as "undamaged structure" in the following. Its height is 800 mm (200 mm for each inter-storey), the plan is squared (300 × 300 mm), the cross section of columns is rectangular (50 × 4 mm) and the one of beams is L-shaped (50 × 50 × 4 mm). A numerical model of the shear-type frame structure was implemented by recognizing 24 significant dofs in the structure (Fig. 1(b)), 6 nodes for each floor (5 on the column and 1 in correspondence with the beam). To implement the numerical model the following values of mass and stiffness coefficients were evaluated from geometry and material properties of structural elements: $m_i = 0,0001773$ N s^2/mm and $m_i = 0,0059923$ N s^2/mm for nodes describing, respectively, the columns and the beams of the structure; $k_i = 3590,33$ N/mm and $k_i = 107189,23$ N/mm for element of floor without and with steel bracing, respectively.

The damage is introduced in the model with a stiffness reduction of the elements. The stiffness k_i^d of the element i interested by the damage can be expressed in relation to the stiffness of the element undamaged, k_i^u, as follows:

$$k_i^d = (1-a)\,k_i^u, \quad i = 1,\dots,n \tag{7}$$

where a is the damage intensity, i.e. $0 \le a < 1$ and $n = 24$ is the number of the elements. Different damage scenarios were considered: damage type "0" confined to a single element (stiffness reduction applied to one element), called D_0^i, where i denotes the ith element; damage type "1" applied to the entire floor (stiffness reduction applied to the six elements of a floor), called D_1^j, where j denotes the jth floor; damage type "2" which involves two consecutive floors (stiffness reduction applied to the twelve elements of two floors), called D_2^{j-k}, where j and k denote the number of the floors. For each type of damage, different damage intensities were considered by assigning to the a parameter the following values: 0.1, 0.3, 0.5. The results reported in Figs. 2–5 are related to damage type "0" of element 5 (D_0^5) and element 22 (D_0^{22}), damage type "1" of floor 2 (D_1^2), damage type "2" of floors 3–4 (D_2^{3-4}). The green area represents the location of damage.

Fig. 2 reports the results of techniques based on dynamic response in time domain (drift variation and curvature variation of deflection profile) which are similar to the results of modal flexibility-based indices determined by applying a positive shear inspection load vector $\mathbf{f} = \{1\}$; Figs. 3–5 represent the results based on frequency domain response obtained through a modal analysis.

In all cases, indices with the best performance are the ones based on drift and curvature variations of deflection profile. COMAC index is able to identify damage location only in the case of damage of i-element, but only if the i-element is not in the first floor (see results of element 5 and element 22). In this case, also RD of the first mode shape gave a good damage position indicator, while RD of the second and third modes did not give good results. For damage on a whole floor and on two consecutive floors, the maximum values of RD were not located in the damaged zone, yet in this area it is possible to observe a more pronounced variation of the index than in the undamaged zone. For the damage on i-element good results were obtained through curvature variation of the first three mode shapes, for the damage on a whole floor through curvature variation of the first two modes and for the damage on two floors through curvature variation of only the first mode.

An overview of these results is given in Table 1, where the indices which correctly locate the damage position are indicated with the check mark "$\surd$", whereas those with a "×" did not provide the correct result.

5. Experimental case study

Experiments have been carried out at the "Laboratory of Materials and Structures" of Sapienza, University of Rome (Italy), on the spatial model of a 4-story shear-type steel described in Section 4 and illustrated in Fig. 1(a). The damage is introduced by removing the bracings and this is indicated as "damaged structure" in the following. By removing the steel bracing a stiffness reduction of the third floor was obtained. Sand (0.3–0.5 mm diameter) was sticked on the structure to create the features to be tracked with the HLPT algorithm and the stochastic pattern to be identified by the DIC algorithm.

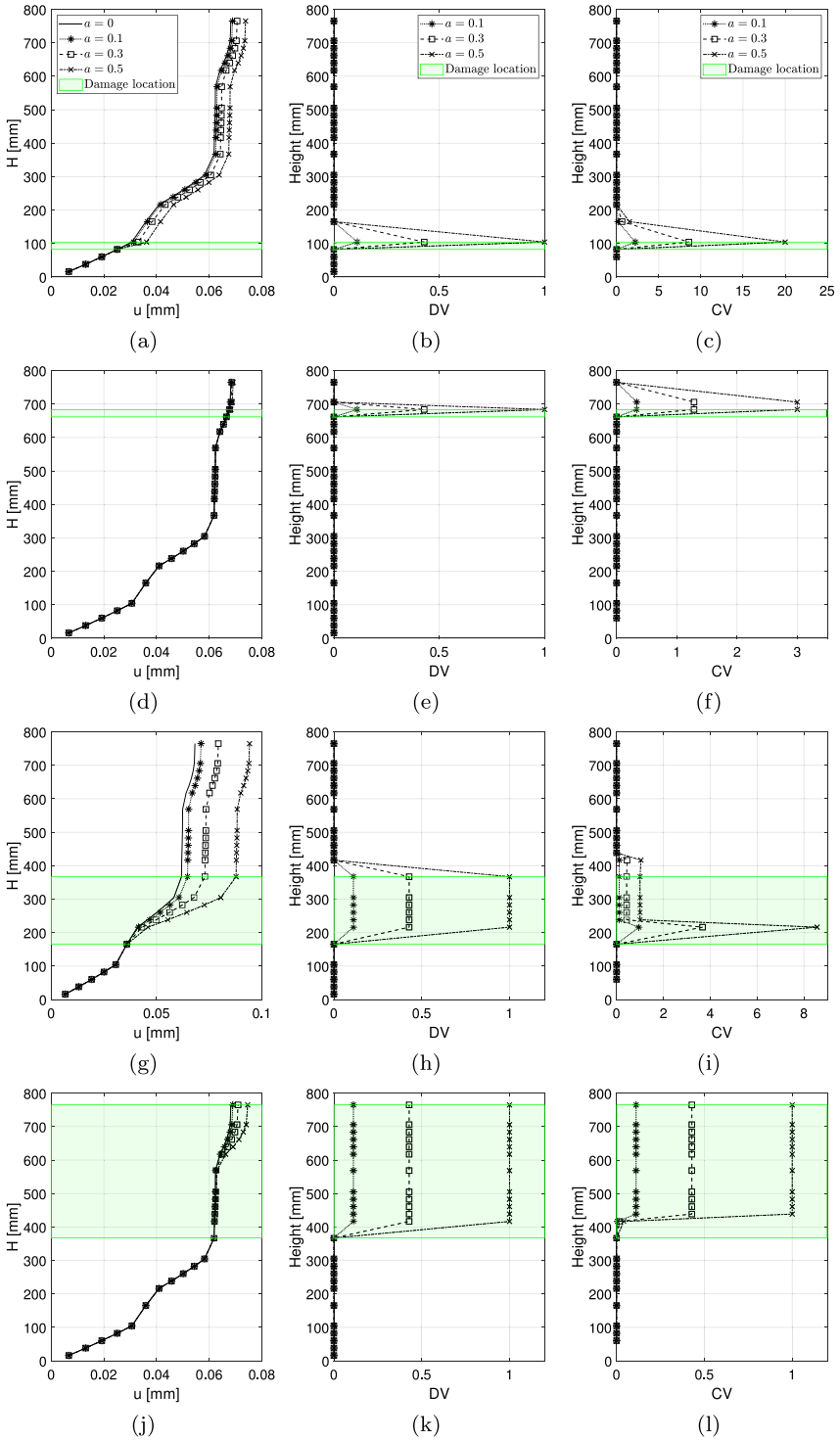

Fig. 2. Deflection profile (u), Drift Variation (DV) and Curvature Variation (CV) for damage D_0^5 (a, b, c), damage D_0^{22} (d, e, f), damage D_1^2 (g, h, i), damage D_2^{3-4} (j, k, l). In each plot, the different lines are related to following values of a parameter, $a = [0.1 \quad 0.3 \quad 0.5]$.

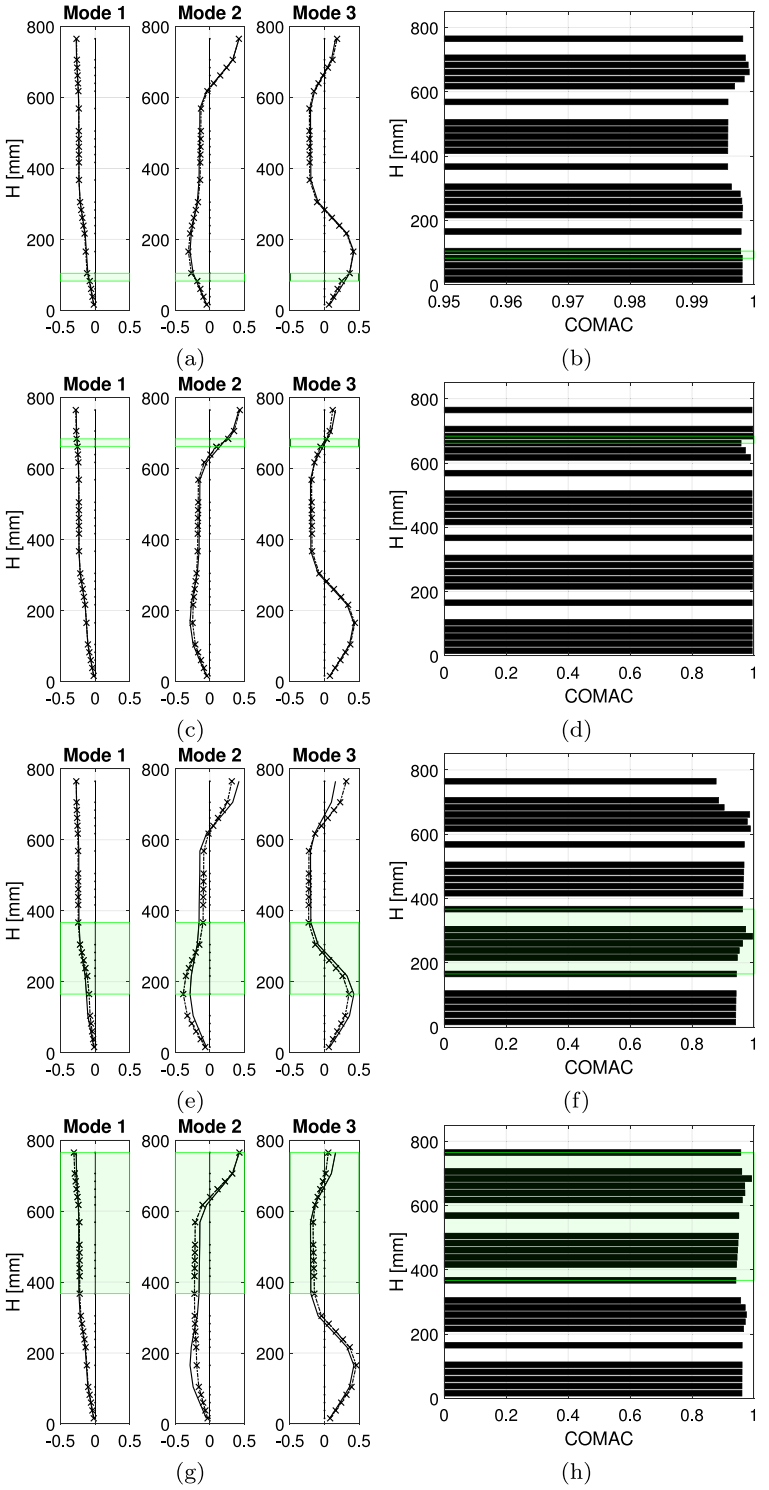

Fig. 3. Mode shapes (undamaged indicated with solid line and damaged with dotted line) and COMAC for damage D_0^5 (a, b), damage D_0^{22} (c, d), damage D_1^2 (e, f), damage D_2^{3-4} (g, h). The damaged state is related to damage parameter $a = 0.5$.

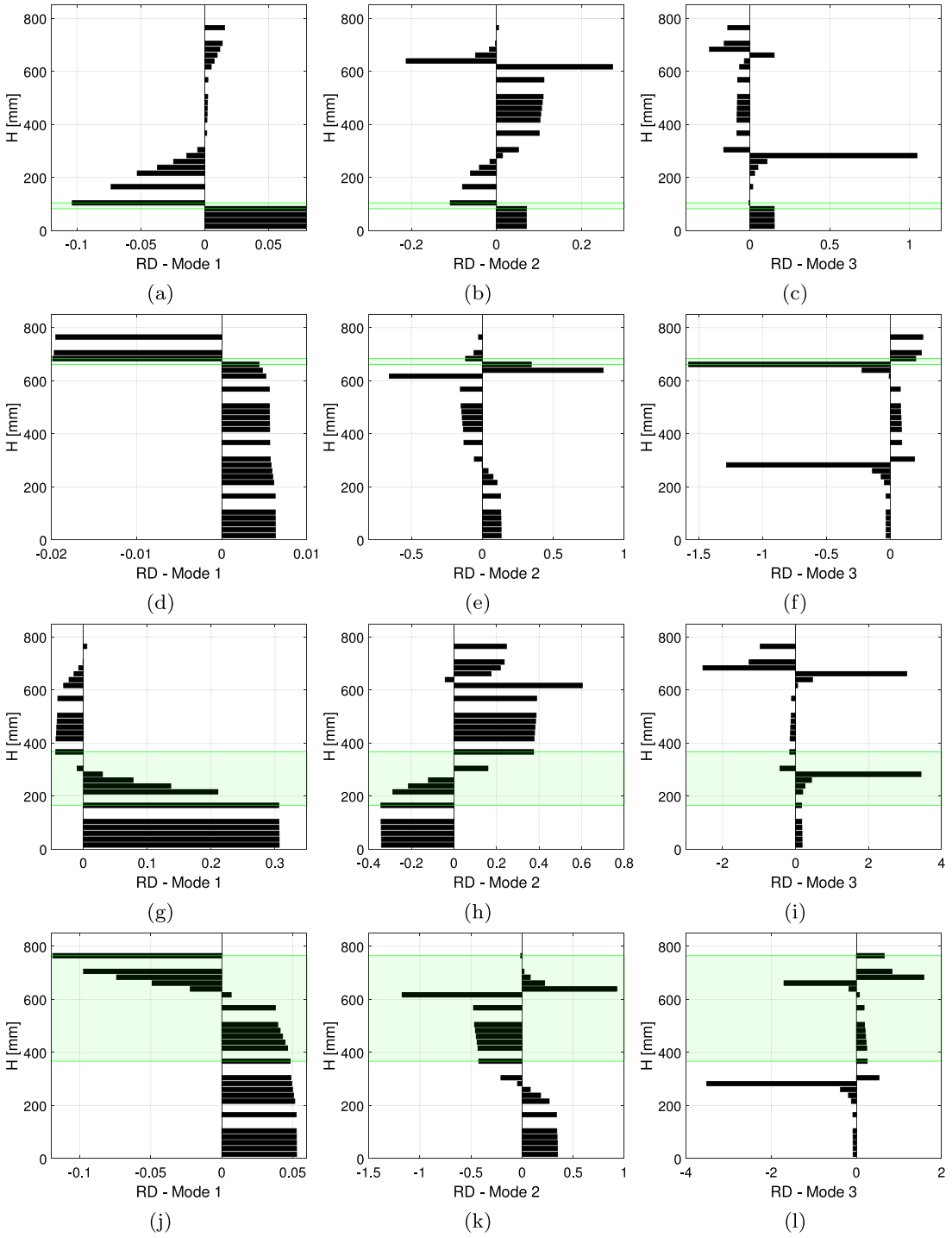

Fig. 4. Mode shapes Relative Difference (RD - Mode 1, Mode 2, Mode 3) related to damaged structure with $a = 0.5$ for damage D_0^5 (a, b, c), damage D_0^{22} (d, e, f), damage D_1^2 (g, h, i), damage D_2^{3-4} (j, k, l).

5.1. Experimental tests and data extraction

Two types of test were conducted, one with a white noise input (flat in the range of the structural frequencies, 8–100 Hz) provided at the base of the structure by an one-dimensional electrodynamical shaker (Dongling GT700M, slip plate dimension

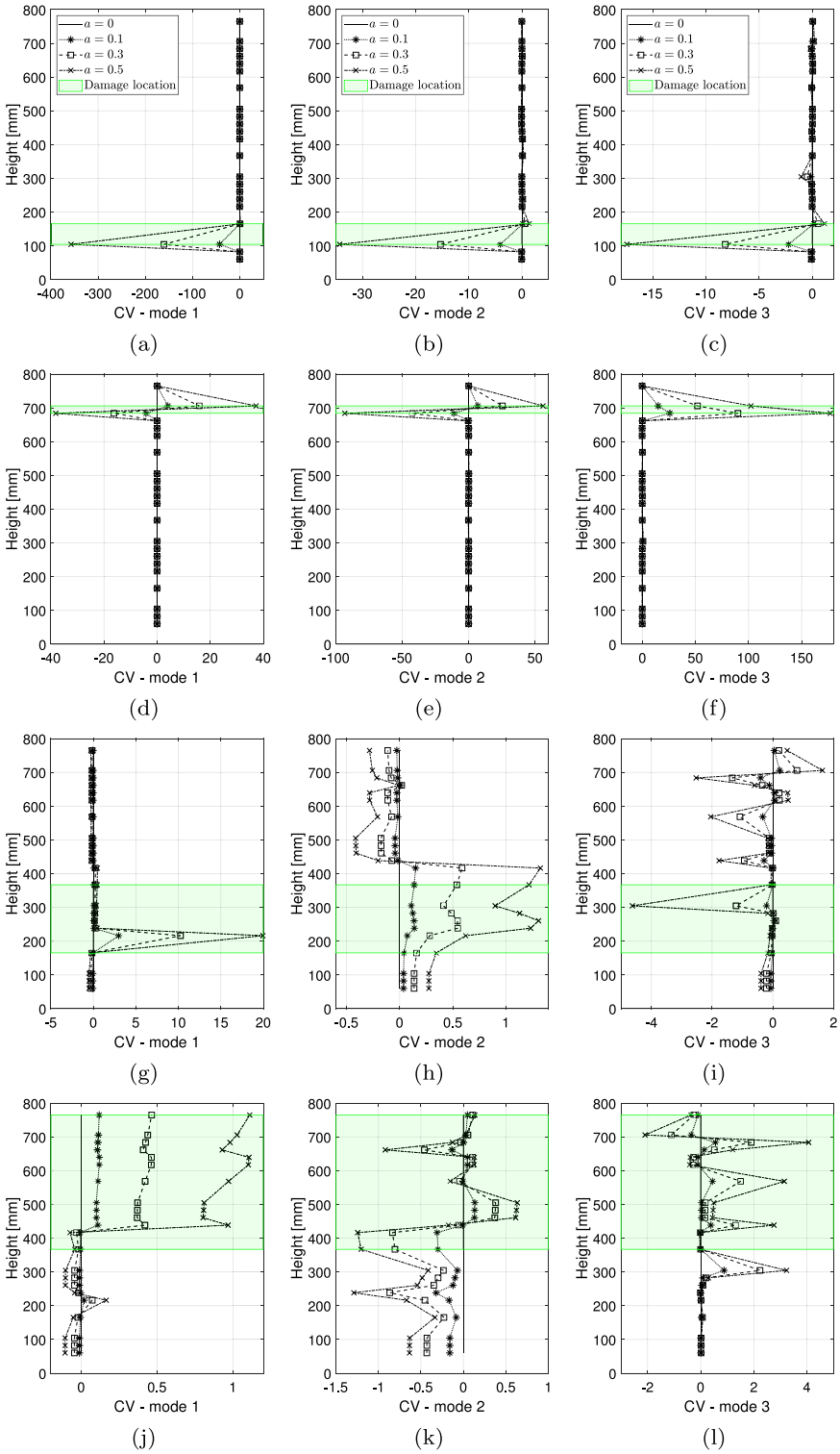

Fig. 5. Mode shapes Curvature Variation (CV - Mode 1, Mode 2, Mode 3) for damage D_0^5 (a, b, c), damage D_0^{22} (d, e, f), damage D_1^2 (g, h, i), damage D_2^{3-4} (j, k, l). In each plot, the different lines are related to following values of a parameter, $a = [0.1 \quad 0.3 \quad 0.5]$.

$700 \times 700 \times 45$ mm^3), and the other with the structure being hit at the top floor with an instrumented hammer (PCB Piezotronics Modally Tuned ICP model, hammer mass 5.5 kg).

Table 1
Summary and comparison of the results of damage location indicators for the numerical case study.

	D_0^5	D_0^{22}	D_1^2	D_2^{3-4}
Techniques based on the dynamic response in the time domain				
Deflection profile at $t = t_{max}$				
▷ Inter-storey Drift Variation (DV)	√	√	√	√
▷ Curvature Variation (CV)	√	√	√	√
Techniques based on modal properties in the frequency domain				
Mode shapes				
▷ Relative Difference (RD)	√	√	×	×
▷ Coordinate Modal Assurance Crit. (COMAC)	×	√	×	×
▷ Curvature Variation (CV)	√	√	√	√
Modal flexibility-based approach				
▷ Inter-storey drift variation (Z index)	√	√	√	√
▷ Curvature Variation (CV)	√	√	√	√

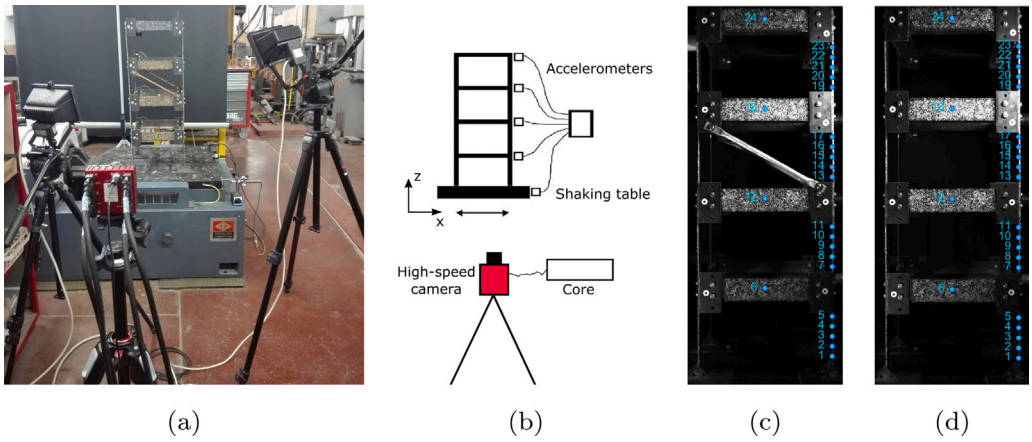

Fig. 6. Experimental setup: (a) the high-speed camera installed in front of the structure to record motion in the plane (x, z); (b) sketch of the experimental setup and reference system; (c, d) measurement points selection on the undamaged and damaged structure respectively.

Two acquisition systems were used to record both accelerometric and image-based measurements. The accelerometers used in these tests were seismic class sensors PCB 393A03 and PCB 352C33 with noise density 2 $\mu g/\sqrt{Hz}$ in the band 1–5000 Hz. The second acquisition system includes a video camera and a digital recorder of IO Industries. The camera is the Flare 12M125xCL, a high resolution, high-speed area scan camera; the resolution is 4096 × 3072 pixels, the pixel size 5.5 μm × 5.5 μm and the frame rate at full resolution is 124 fps (8-bit) and 100 fps (10-bit). For this experiments, the frame rate of the camera was set to 200 fps with 320 × 763 pixel the size of the image. The digital recorder is the CORE2CLPLUS IO DVR, Core 2. The camera was installed in front of the structure to capture images in the motion plane, as sketched in Fig. 6. Further details on the experimental setup are reported in [36].

The algorithms used to process the high-speed camera images return the trajectories of feature points (stochastic pattern), created by attaching sand on beams and columns surfaces. Different points have been sampled along the whole structure obtaining many more measurement points than the accelerometer system acquisition. The comparison between the two image analysis techniques is showed in Fig. 7 for a test in which the structure is excited through an hammer and in Fig. 8 for which a shaker test is considered. The results are compared in terms of displacement time histories of fourth floor (dof 4), as reported in Fig. 7(a, b) and Fig. 8(a, b), Power Spectral Density (PSD) depicted in Fig. 7(c) an Fig. 8(c), and mode shapes identified from the image-based signals showed in Fig. 7(d) an Fig. 8(d). Furthermore, in Table 2 a computational time comparison is reported; the image analyses have been performed on a Corei7-8th Gen Intel® CPU laptop, with 16 GB memory.

Although the results of the feature extraction are practically the same either in terms of time series or power spectra, the DIC algorithm was 2 times faster on the laptop computer used for the test. Therefore, all the subsequent analyses are carried out with DIC data.

5.2. Image based operational modal analysis

Operational modal analysis (OMA) allows to describe structural dynamics in real operating conditions with unknown excitation. The advantages and drawbacks of such output-only techniques are discussed in [37] where they are applied to extract useful

Table 2
Image analysis computational time carried out on a Corei7-8th Gen Intel® CPU laptop, with 16GB memory.

	Test duration	Visual tracking duration	
		HLPT	DIC
Shaker test	110 s	5 h	2 h
Hammer test	14 s	2 h	1 h

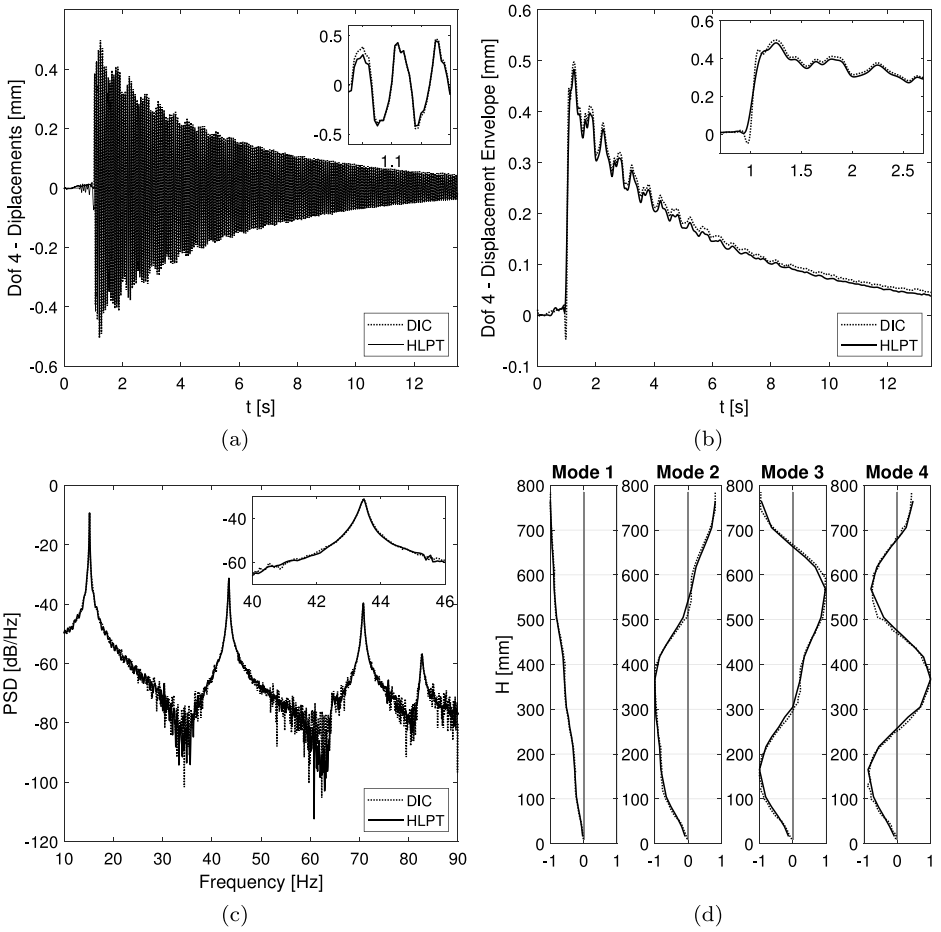

Fig. 7. Results of the hammer test executed on the damaged structure obtained with HLPT (solid line) and DIC algorithm (dotted line): (a) Displacement time histories of the fourth floor; (b) Displacement envelope; (c) Power Spectral Density (PSD); (d) Mode shapes.

information from rapid dynamic testing of seismically damaged complex buildings. Different procedures, such as Enhanced Frequency Domain Decomposition (EFFD), Eigensystem Realization Algorithm (ERA), Stochastic Subspace Identification (SSI), and Time–Frequency Instantaneous Estimators (TFIE), for identifying both modal and physical models for output-only modal identification are discussed in [38] and their performance are evaluated with the ambient vibration response of a three-dimensional frame structure.

In our work, modal properties of the structure in the undamaged and damaged configuration have been extracted by the Frequency Domain Decomposition (FDD) [39] and Stochastic Subspace Identification (SSI) [40] techniques applied to the results of the white-noise shaker test.

These analysis were conducted by using the displacements obtained by the DIC algorithm for 24 measurement points chosen by the authors and shown in Fig. 6(c, d) (for each floor, the column was divided in five areas and the beam in one area; the selected points are in the centre of such areas). In addition, 4 accelerometer, one at each floor, were used as comparison.

The natural frequencies identified with these techniques are listed in Table 3 for both undamaged and damaged structure. Fig. 9 reports the mode shapes identified with FDD and Fig. 10 reports the stabilization diagrams obtained by applying SSI. The natural frequencies identified with SSI from the accelerograms and the image based displacements differ by less than 3% and the ones

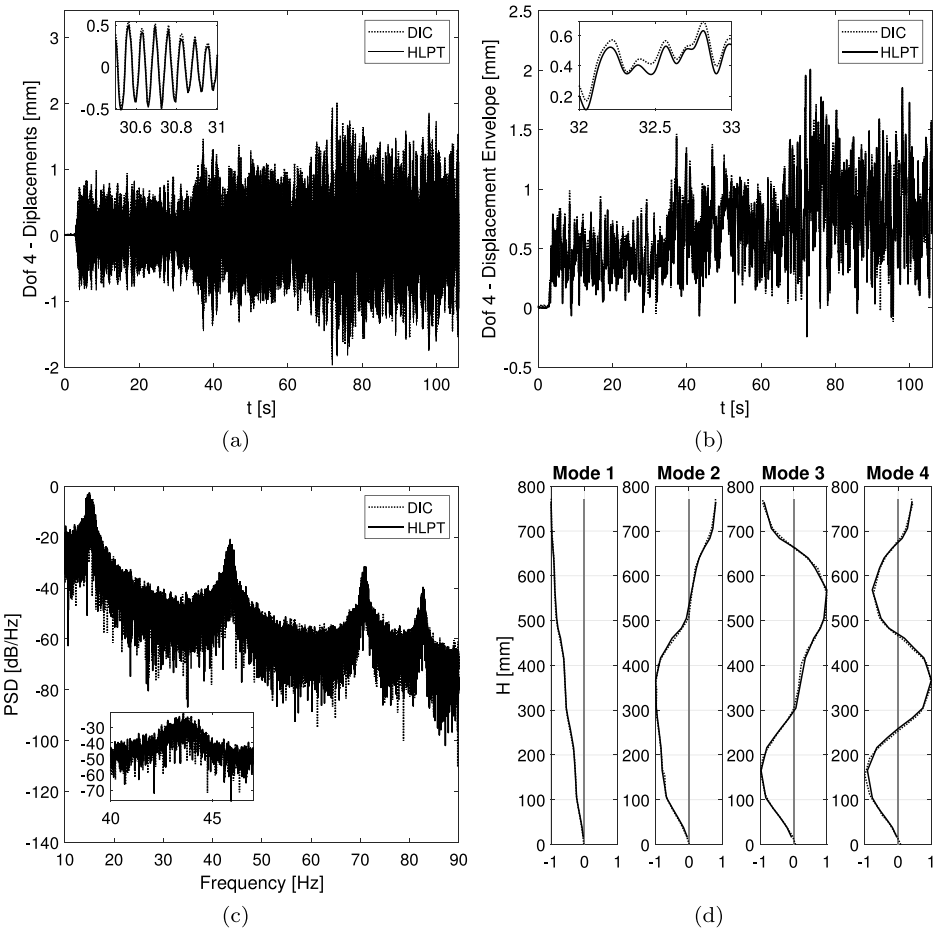

Fig. 8. Results of the white noise test executed on the damaged structure obtained with HLPT (solid line) and DIC algorithm (dotted line): (a) Displacement time histories of the fourth floor; (b) Displacement envelope; (c) Power Spectral Density (PSD); (d) Mode shapes.

Table 3
Modal frequencies extracted through SSI and FDD techniques and from acceleration and displacement measurements.

	Undamaged structure				Damaged structure			
	Acceleration		Displacement		Acceleration		Displacement	
Mode	SSI [Hz]	FDD [Hz]	SSI [Hz]	FDD [Hz]	SSI [Hz]	FDD [Hz]	SSI [Hz]	FDD [Hz]
1	16,7	17,3	17,2	17,2	14,6	14,9	15,1	14,9
2	53,8	54,9	54,9	55,0	42,9	43,9	43,5	43,58
3	71,5	72,9	72,8	72,9	69,5	71,0	70,8	71,1

identified with FDD differ by less than 1%; the image-based mode shapes evaluation is more accurate than the accelerometric one thanks to the higher number of measurement points available.

5.3. Damage location

The focus of this section is the use of the results of the image-based OMA in damage detection procedures. To tackle this problem, several techniques will be compared both in the time and in the frequency domains and the results will allow to highlight advantages and disadvantages of each technique in terms of accuracy in determining damage location and damage intensity. For example, in [41] two approaches have been used for the monitoring of dynamic systems. Both are based on stochastic subspace identification and take the statistical uncertainties into account. One approach requires a statistical damage indicator to automatically evaluate changes in the structural response without computing any modal parameters and the other approach requires modal parameter and their confidence intervals estimate.

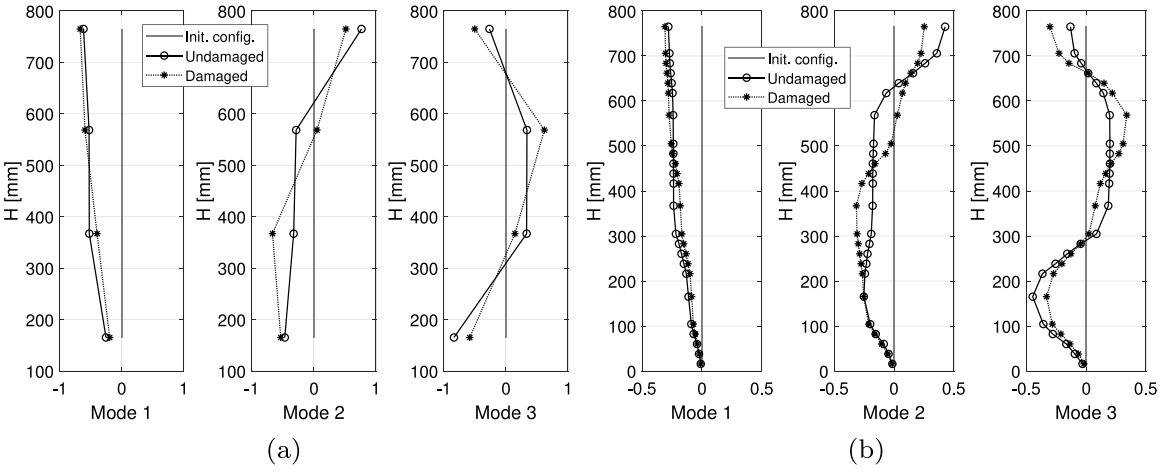

Fig. 9. Mode shapes extracted through the FDD technique from acceleration (a) and displacement (b) measurements.

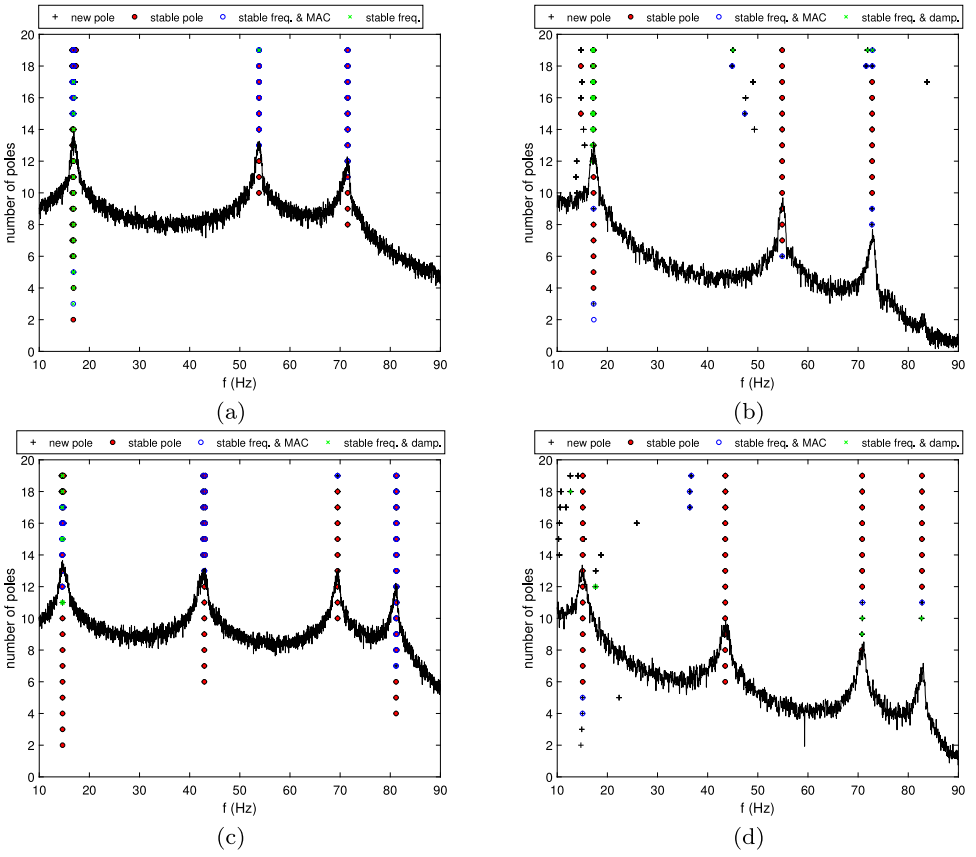

Fig. 10. Stochastic Subspace Identification (SSI): stabilization diagrams for undamaged and damaged structure from acceleration (a,c) and displacement (b,d) measurements.

As previously described, the determination of the position of damage in the structure can be pursued by methods belonging to the time domain and frequency domain categories. Both approaches are followed to evaluate their performance in the experimental case study. The location of the damage is achieved by selecting the area where the damage indices exceed a fixed threshold. Thresholds were chosen from the numerical sensitivity analysis carried out in Section 4. In particular, the two "extreme" damage cases (stiffness

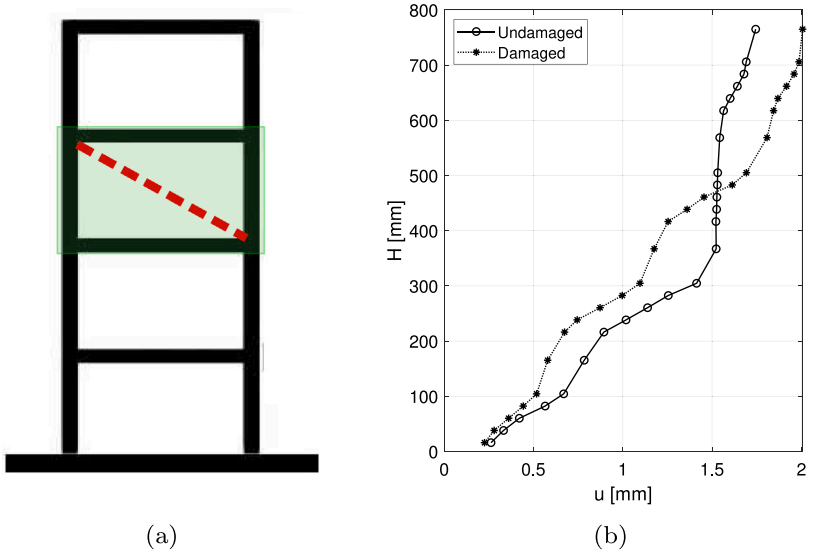

Fig. 11. Time-based damage identification methods: (a) area of the structure, evidenced in green, interested by the damage; (b) maximum deflection of the structure recorded at $t = t_{\max}$.

reduction of 10% and 90%) were used as best and worst case scenarios with the corresponding indicators called $I_{0.1}$ and $I_{0.9}$. The threshold was chosen to be:

$$I^{\text{thr}} = I_{0.1} + 0.15\,(I_{0.9} - I_{0.1}). \tag{8}$$

5.3.1. Techniques based on the dynamic response in the time domain

An effective damage index, based on displacement measurements, is the inter-storey drift. In this context, the use of high-speed camera offers the advantage of a direct measurement of displacement without the need of integrating twice the acceleration to obtain a direct measurement of the displacement. The corresponding deflection of undamaged and damaged structures under white noise excitation is shown in Fig. 11.

The results in Fig. 12(b) show that the highest values of the DV are located at an height between $400 \div 600$ mm which actually coincides with the inter-storey 2–3 where the steel bracings were removed.

The large amount of measurement points made available through the image analysis technique allowed us to evaluate the curvature of the deflection profile (Fig. 12(c)) of the structure and to use the Curvature Variation (CV) as an additional damage index. Fig. 12(d) shows also the CV is localized in the region where damage occurred. However, when compared to DV the damage is concentrated on a narrow region.

5.3.2. Techniques based on modal properties in the frequency domain

In Fig. 13 both the RD and COMAC indices are evaluated for the mode shapes obtained for the acceleration data ($N = 4$) and the displacement data ($N = 24$). When considering the RD index, acceleration and displacement data gave the similar results only for the first mode for which the maxima are obtained at the same location (see the grey and the black bars in Fig. 13(a)). For the second and third mode the maximum absolute value of RD evaluated with displacement measurements is located in the range $600 \div 700$ mm, while the maximum values of RD evaluated with acceleration measurements are in the range $350 \div 600$ mm. In all cases, RD index failed to provide a clear indication of the damage position. The minimum values of COMAC are in the range $350 \div 600$ for acceleration measurements while for the displacement ones there are three local minima in the range $350 \div 800$ where also two maxima appear. It is noted that the large number of measurement points offered by image analysis does not provide any significant advantage in terms of damage localization when compared to the few measurement points of the acceleration data.

The accuracy in mode shape estimate made possible by the large number of measurement points favours modal shapes and modal curvatures based identification techniques. The signals recorded during the test was divided in 20 intervals, 10 for the undamaged state and 10 for the damaged stare, and for each interval, natural frequencies and mode shapes were evaluated. In Fig. 14 the CV of the mode shape profiles evaluated for each interval is reported. The highest values of the CV are located in the range $400 \div 600$ mm for the mode shapes 1 and 2, while the CV of mode shape 3 has high values in the range $400 \div 800$ mm. Yet in all cases, the maximum variations is obtained in the damaged region at least for lower order modes. For higher modes, CV have spurious peaks which have to be filtered out [42,43].

The results of the approach based on the damage-induced deflections estimated by modal flexibility from ambient vibration measurements are showed in Fig. 15. The Z-index for both acceleration and displacement measurements was evaluated. The signals recorded during the test performed on the undamaged structure was divided in 10 intervals; at each interval, natural frequencies,

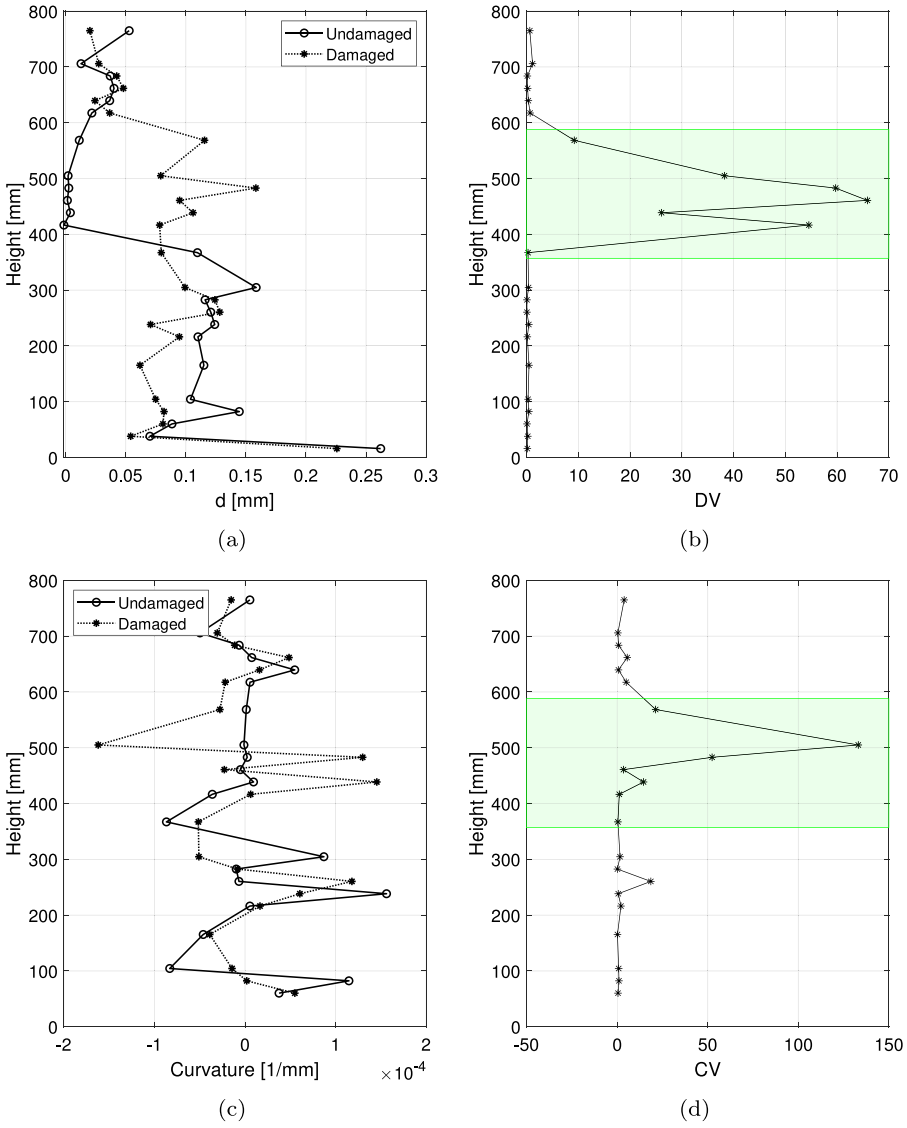

Fig. 12. Time-based damage identification methods: (a) inter-storey drift at $t = t_{max}$; (b) inter-storey Drift Variation at $t = t_{max}$; (c) curvature at $t = t_{max}$; (d) Curvature Variation at $t = t_{max}$.

mode shapes and deflection profile under a positive shear inspection were evaluated. Then, the mean value and the standard deviation of d_i^u were computed, by considering the undamaged state data as a training data set.

The maximum values of the Z-index occur in the range $400 \div 600$ mm of the height of the structure that corresponds to the zone where the steel bracings have been removed. Both measurements return a good estimate of damage localization but thanks to the larger number of measurement points provided by image analysis it is possible to assess that the damage affects all the zone between 400 and 600 mm, while with the acceleration acquisition system it is possible to individuate only one point affected by damage (corresponding to the sensor on the third floor).

In Fig. 16 the CV of the deflection profile obtained with the modal-flexibility approach is reported. The highest values of the CV are located in the range $400 \div 600$ mm for the case of deflection profile.

Indeed, the CV damage index is more accurate if applied to the actual deflection profile for an assigned instant of time (Fig. 12(d)) and to the deflection profile obtained with the modal flexibility approach (Fig. 16(c)), rather than to the mode shapes profile (Fig. 14).

An overview of the effectiveness of each damage index is given in Table 4. Consistently with the numerical case study, the indices which correctly locate the damage position are indicated with the check mark "$\surd$", whereas those with a "×" did not provide the correct result. Furthermore, the symbol "-" is used when it was not possible to calculate the indicator with that type of measurements. The direct displacement measurements allow to use techniques based on the deformation of the structure at a certain instant of

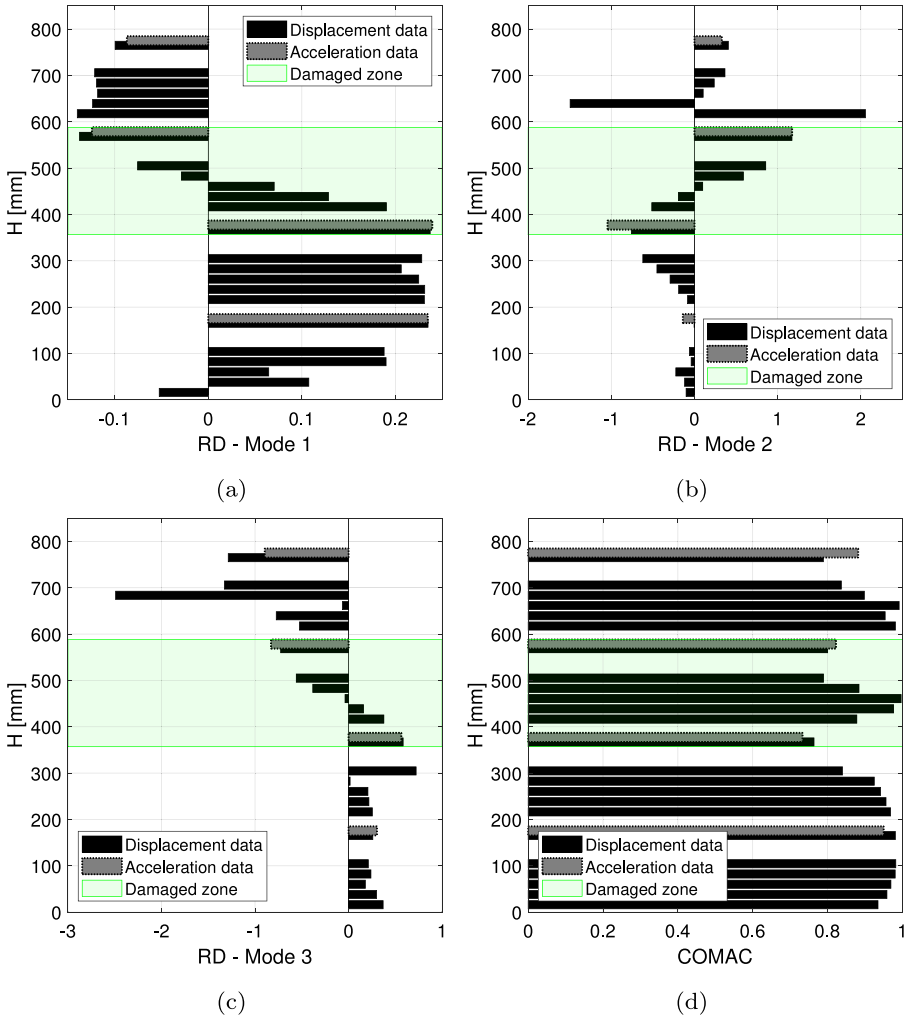

Fig. 13. Relative Difference (a, b, c) and COordinate Modal Assurance Criteria (d) evaluated with acceleration and displacement measurements.

time and those based on the variation of curvature. The RD and COMAC indices give better results in the case of accelerometric measurements, while the drift-based indices are able to localize the damage both by accelerometric and displacement measurements but with the latter a more accurate localization was obtained. These experimental results are consistent with numerical simulations carried out by considering the damage type of an entire floor, D_1^j. Indeed, by comparing the *Displacements* in Table 4 with the D_1^2 of Table 1, it is seen that the indices computed through displacement give the same results of those evaluated in the numerical case study in terms of the capability of locating the damage.

5.4. Damage intensity

The methods described in the previous section allow the localization of damage. In this section, those results are used to solve the inverse problem related to the estimate of the damage intensity. Such an approach requires numerical model of the structure and a comparison between its undamaged and damaged state; as such, two numerical models of the shear-type frame structure have been implemented, a 4-dofs and a 24-dofs modal model (Fig. 1(b)) to assess the damage intensity by using, respectively, accelerometer and image-based measurements. The first model was obtained by recognizing 4 significant dofs in the structure, which are the 4 horizontal translations of each floor for the shear-type frame; the second model was implemented with 24 dofs (as described in Section 4), in analogy to the displacement measurement points. These models were used to evaluate the natural frequencies f_j and to extract the corresponding mode shapes.

After identifying the location of the damage by selecting the area where the indices reported in the previous section exceed the fixed threshold, the damage is introduced in the model with a stiffness reduction of the elements which are situated in the localization area. The stiffness k_i^d of the element i interested by the damage can be expressed in relation to the stiffness of the element undamaged, k_i^u, according to the Eq. (7), by considering $n = 4$ and $n = 24$ for 4-dofs and 24-dofs model respectively.

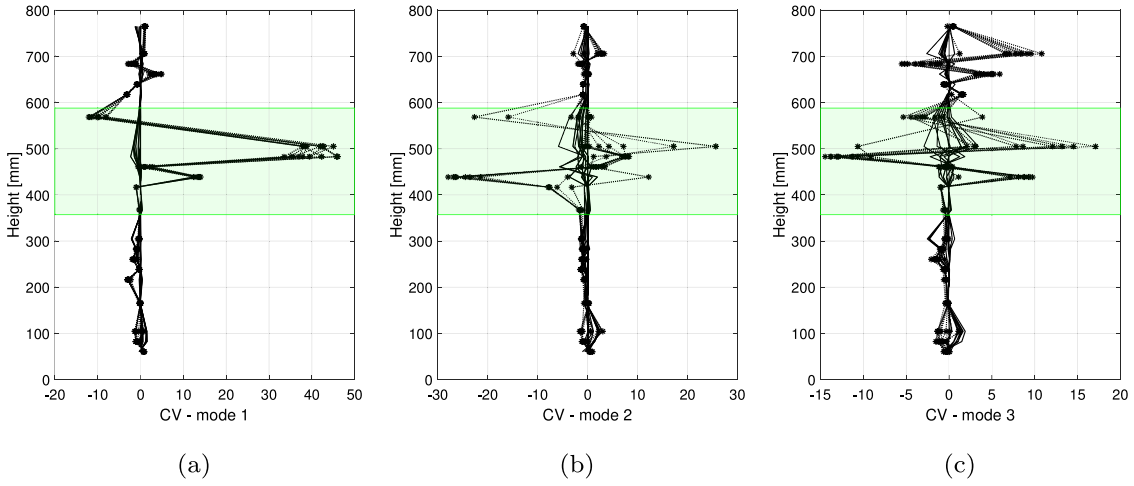

Fig. 14. Modal curvature-based approach applied to displacement measurements: Curvature Variation of mode 1 (a), mode 2 (b), mode 3 (c). Solid line for the undamaged state, dotted line for the damaged one. The signals recorded during the test on the undamaged and damaged structure were divided in 10 intervals, respectively; at each interval, mode shapes and their CV were evaluated.

Table 4
Summary and comparison of the results of damage location indicators.

	Accelerations	Displacements
Techniques based on the dynamic response in the time domain		
Deflection profile at $t = t_{max}$		
▷ Inter-storey Drift Variation (DV)	–	√
▷ Curvature Variation (CV)	–	√
Techniques based on modal properties in the frequency domain		
Mode shapes		
▷ Relative Difference (RD)	√	×
▷ Coordinate Modal Assurance Crit. (COMAC)	√	×
▷ Curvature Variation (CV)	–	√
Modal flexibility-based approach		
▷ Inter-storey drift variation (Z index)	√	√
▷ Curvature Variation (CV)	–	√

The estimate of the parameter a constitutes the assessment of the damage intensity. An optimal estimate of this parameter can be obtained by minimizing an objective function based on the sum of difference between numerical $\Delta f_j(a)$ and experimental Δf_{ej} frequencies variation from undamaged to damaged state, i.e.,

$$G(a) = \sum_{j=1}^{L} \left(\frac{\Delta f_j(a)}{f_j^u} - \frac{\Delta f_{ej}}{f_{ej}^u} \right)^2 \tag{9}$$

where L denotes the number of the identified modes, $\Delta f_j(a) = f_j^u - f_j^d(a)$ and $\Delta f_{ej} = f_{ej}^u - f_{ej}^d$.

The G function is calculated in Fig. 17 for experimental frequencies obtained from accelerometer and image-based measurements after having identified the location of the damage with the methods previously presented. The actual damage intensity is represented with a vertical dashed line. In this figure, they are classified differently from the classification of the previous section. In Fig. 17(a) is reported the objective function coming from a pre-localization of the damage based on drift variation: DV at t_{max} (Fig. 12(b)) and Z-index from modal flexibility-based approach (Fig. 15(c, f)). In Fig. 17(b) the pre-localization is obtained with curvature variation indices: CV at t_{max} (Fig. 12(d)), CV of mode shapes Fig. 14 and CV from modal flexibility-based approach (Fig. 16(b)). Fig. 17(c, d) report the results coming from a damage located with COMAC (Fig. 13(d)) and RD (Fig. 13(a, b, c)) index, respectively.

These results show that the only the damage indices based on drift variation (17(a)) allow to obtain a good assessment of damage intensity: only in this case, in fact, the value of the parameter a that minimize of $G(a)$ coincides with the actual value of the a (indicated by the dashed line). In all other cases, the stiffness reduction is underestimated by at least 15%.

6. Conclusions

In this work, two vision-based techniques were used to measure the dynamic displacements of a small-scale frame structure and to extract its modal properties. The advantages of these contactless measurements are discussed in terms of capability of detecting

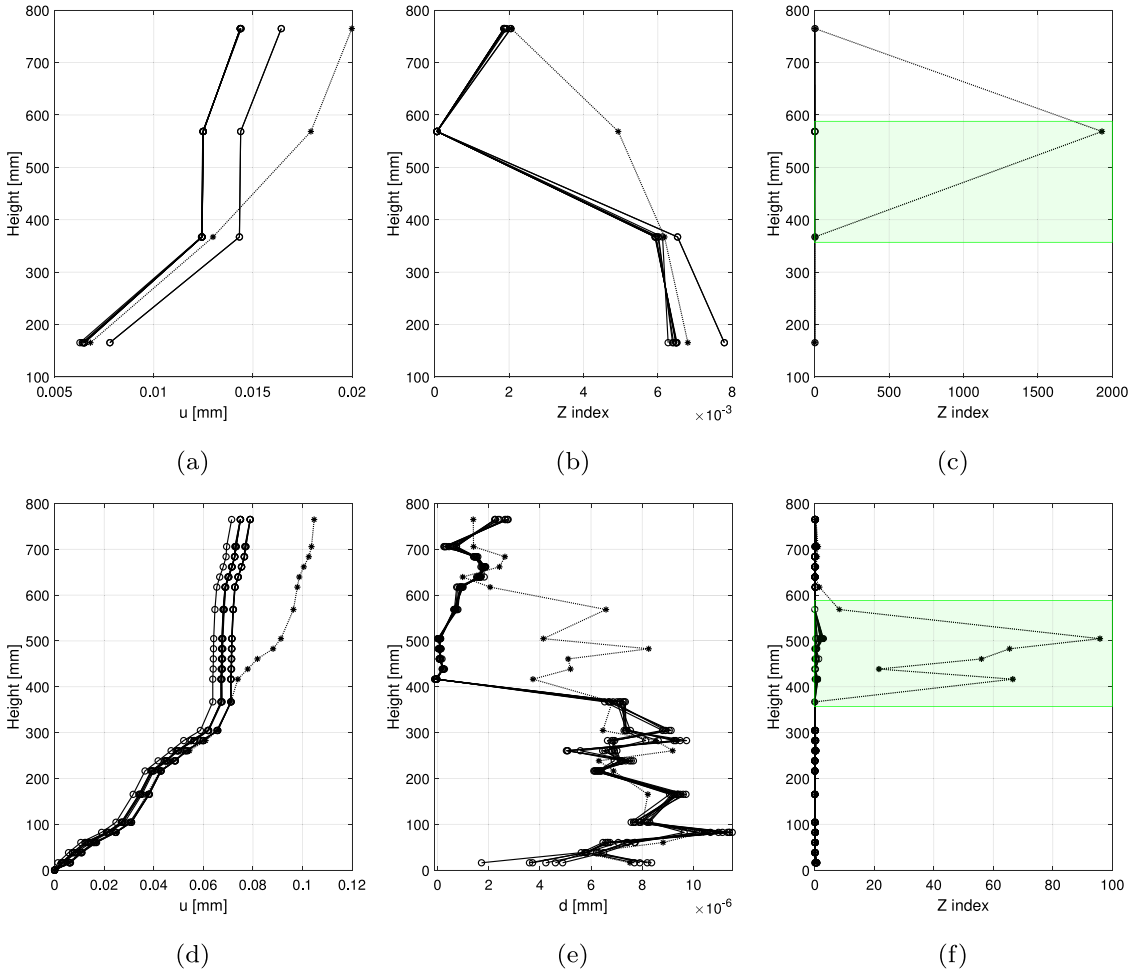

Fig. 15. Modal flexibility-based approach applied to acceleration (a, b, c) and displacement (d, e, f) measurements: deflection (a, d), inter-storey drift (b, e), Z-index (c, f). Solid line for the undamaged state, dotted line for the damaged one. The signals recorded during the test on the undamaged and damaged structure were divided in 10 intervals, respectively; at each interval, deflection profile under a positive shear inspection and the corresponding Z index were evaluated.

structural damages. Numerical experiments on damage localization were carried out to take into account different type and intensity of damage and to evaluate the performance of both techniques based on dynamic response in time domain and techniques based on mode shapes in the frequency domain.

In the experimental case of study one type of damage was considered by removing the steel brace of the third floor. The displacements extracted from the image analysis were processed to obtain the dynamic features either in the time domain and in the frequency one. In general, it is shown that having a much larger number of measurement points allows a more accurate assessment of the damage position, although for some of the considered techniques these advantages were not apparent. In particular the COMAC and RD indices used with a large number of measurement points gave many false positives. On the other hand, those indices that make use of variations along the structure greatly benefit from the number of tracked points, resulting in a much clearer indication of the damage position, as in the case of the Z index. These results were consistent with the numerical simulations carried out by considering the damage of an entire floor.

The damage intensity was assessed with a procedure based on the pre-localization and on the definition of an inverse problem, which required the implementation of a numerical model of the structure. The optimization problem was solved by minimizing the distance between numerical and experimental frequency variations from undamaged and damaged states. The results showed that, among all considered techniques, only two (Z-index and DV) allowed an accurate assessment of the intensity. This was certainly due to the good prelocalization offered by these indices which made the inverse problem locally convex.

To conclude, it has been shown that damage detection algorithms can greatly improve by using the large number of measurement points made available by image-based operational modal analysis.

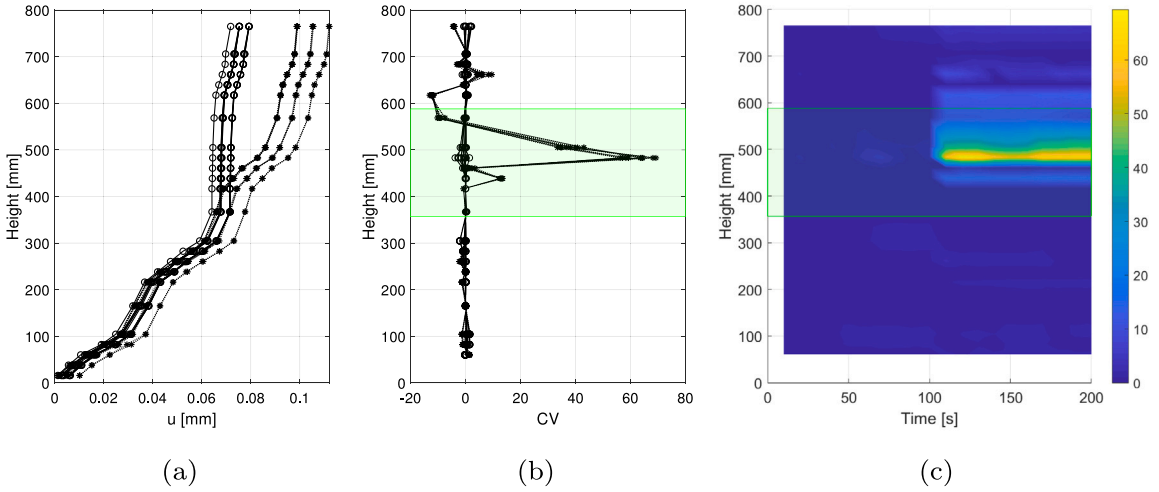

Fig. 16. Modal flexibility-based approach applied to displacement measurements: deflection (a), Curvature Variation of the deflection profile (b), Curvature Variation in time (c). Solid line for the undamaged state, dotted line for the damaged one. The signals recorded during the test on the undamaged and damaged structure were divided in 10 intervals, respectively; at each interval, deflection profile and its CV were evaluated.

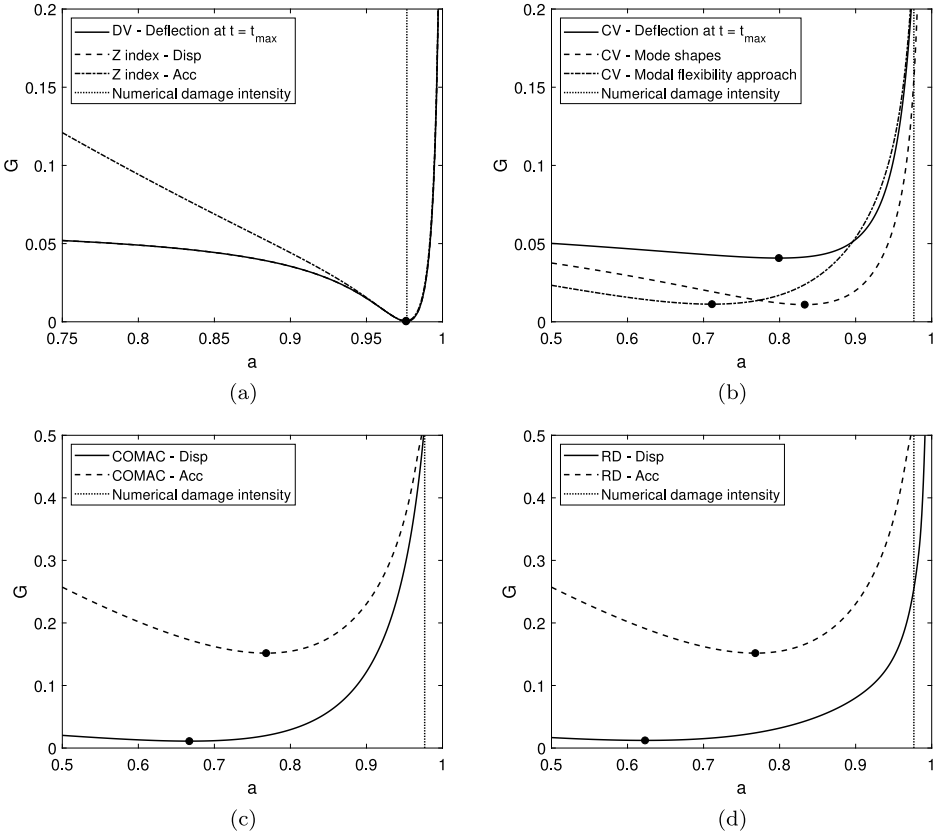

Fig. 17. The objective function $G(a)$ calculated with experimental frequencies obtained from accelerometer (Acc) and image-based (Disp) measurements after identifying the location of the damage with different methods, based on drift variation (a), curvature variation (b), COMAC (c) and RD (d).

CRediT authorship contribution statement

Cecilia Rinaldi: Data curation, Software, Writing – original draft, Visualization. **Jacopo Ciambella:** Conceptualization, Investigation, Validation, Writing – review & editing. **Vincenzo Gattulli:** Conceptualization, Methodology, Funding acquisition.

Declaration of competing interest

Vincenzo Gattulli reports financial support was provided by Research Fund for Coal and Steel.

Acknowledgements

This work is part of a project that has received funding from the EU programme RFCS - Research Fund for Coal and Steel, EU - under grant agreement No 800687.

References

[1] X.W. Ye, C.Z. Dong, T. Liu, A review of machine vision-based structural health monitoring: methodologies and applications, J. Sensors 2016 (2016).
[2] D. Feng, M. Feng, Computer vision for SHM of civil infrastructure: From dynamic response measurement to damage detection – review, Eng. Struct. 156 (2018) 105–117.
[3] B.F. Spencer Jr., V. Hoskere, Y. Narazaki, Advances in computer vision-based civil infrastructure inspection and monitoring, Engineering 5 (2) (2019) 199–222.
[4] C.Z. Dong, F.N. Catbas, A review of computer vision–based structural health monitoring at local and global levels, Struct. Health Monit. 20 (2) (2020) 692–743.
[5] A. Zona, Vision-based vibration monitoring of structures and infrastructures: An overview of recent applications, Infrastructures 6 (1) (2021) 4.
[6] J.G. Chen, N. Wadhwaa, Y.J. Cha, F. Durand, W.T. Freeman, O. Buyukozturk, Modal identification of simple structure swith high-speed video using motion magnification, J. Sound Vib. 345 (2015) 58–71.
[7] J. Guo, J. Jiao, K. Fujita, I. Takewaki, Damage identification for frame structures using vision-based measurement, Eng. Struct. 199, 109634 (2019).
[8] H.Y. Chang, F.G. Yuan, Visualization of hidden damage from scattered wavefield reconstructed using an integrated high-speed camera system, Struct. Health Monit. (2020) 1475921720940805.
[9] P. Olaszek, Investigation of the dynamic characteristic of bridge structures using a computer vision method, Measurement 25 (3) (1999) 227–236.
[10] H. Yoon, H. Elanwar, H. Choi, M. Golparvar-Fard, B.F.S. Jr., Target-free approach for vision-based structural system identification using consumer-grade cameras, Struct. Control Health Monit. 23 (2016) 1405–1416.
[11] C. Harris, M. Stephens, A combined corner and edge detector, in: Alvey Vision Conference, 1988. Manchester, UK.
[12] C. Tomasi, T. Kanade, Detection and tracking of point features, in: School of Computer Science, Carnegie Mellon Univ: Pittsburgh, 1991.
[13] Y. Xu, Photogrammetry-based structural damage detection by tracking a visible laser line, Struct. Health Monit. 19 (1) (2020) 322–336.
[14] A. Havaran, M. Mahmoudi, Extracting structural dynamic properties utilizing close photogrammetry method, Measurement 150 (2020) 107092.
[15] Y. Yang, C. Dorn, T. Mancini, Z. Talken, G. Kenyon, C. Farrar, D.M. nas, Blind identification of full-field vibration modes from video measurements with phase-based video motion magnification, Mech. Syst. Signal Process. 85 (2017) 567–590.
[16] Y.F. Ji, C.C. Chang, Nontarget image-based technique for small cable vibration measurement, J. Bridge Eng. 13 (1) (2008) 34–42.
[17] S. Patsias, W.J. Staszewskiy, Damage detection using optical measurements and wavelets, Struct. Health Monit. 1 (1) (2002) 5–22.
[18] U.P. Poudel, G. Fu, J. Ye, Structural damage detection using digital video imaging technique and wavelet transformation, J. Sound Vib. 286 (4-5) (2005) 869–895.
[19] D.M. McCarthy, Monitoring 3D vibrations in structures using high resolution blurred imagery, (Ph.D. thesis), School of Civil and Building Engineering Loughborough University, 2015.
[20] G. Boracchi, V. Caglioti, A. Giusti, Ball position and motion reconstruction from blur in a single perspective image, in: Image Analysis and Processing, 2007. ICIAP 2007. 14th International Conference, IEEE Comput. Soc., Iciap, Modena.
[21] D.M.J. McCarthy, J.H. Chandler, A. Palmeri, Monitoring dynamic structural tests using image deblurring techniques, Key Eng. Mater. (2013) 932–939.
[22] S. Yoneyama, G. Murasawae, Digital image correlation, in: J. Freire (Ed.), Experimental Mechanics, in: Encyclopedia of Life Support System (EOLSS), Oxford, UK, 2009.
[23] M. Moroni, A. Cicci, M. Bravi, Experimental investigation of a local recirculation photobioreactor for mass cultures of photosynthetic microorganisms, Water Res. 52 (2014) 29–39.
[24] B. Pan, L. Tian, X. Song, Real-time, non-contact and targetless measurement of vertical deflection of bridges using off-axis digital image correlation, Ndt E Int. 79 (2016) 73–80.
[25] A. Khaloo, D. Lattanzi, Pixel-wise structural motion tracking from rectified repurposed videos, Struct. Control Health Monit. 24 (11) (2017) e2009.
[26] H. Yoon, H. Elanwar, H. Choi, M. Golparvar-Fard, B.F. Spencer Jr., Target-free approach for vision-based structural system identification using consumer-grade cameras, Struct. Control Health Monit. 23 (12) (2016) 1405–1416.
[27] J. Cattarius, D.J. Inman, Time domain analysis for damage detection in smart structures, Mech. Syst. Signal Process. 11 (3) (1997) 409–423.
[28] M. Vafaei, A.B. Adnan, A.B.A. Rahman, Real-time seismic damage detection of concrete shear walls using artificial neural networks, J. Earthq. Eng. 17 (1) (2013) 137–154.
[29] M. Celebi, A. Sanli, M. Sinclair, S. Gallant, D. Radulescu, Real-time seismic monitoring needs of a building owner—and the solution: A cooperative effort, Earthq. Spectr. 20 (2) (2004) 333–346.
[30] A.S. Hokmabadi, B. Fatahi, B. Samali, Recording interstorey drifts of structures in time-history approach for seismic design of building frames, Aust. J. Struct. Eng. 13 (2) (2012) 175–180.
[31] C.H.J. Fox, The location of defects in structures. A comparison of the use of natural frequency and mode shape data, in: 10th International Modal Analysis Conference, IMAC, 1992.
[32] N.A.J. Lieven, D.J. Ewins, Spatial correlation of mode shapes, the coordinate modal assurance criterion (COMAC), in: 6th International Modal Analysis Conference, IMAC, 1998.
[33] J. Ciambella, A. Pau, F. Vestroni, Effective filtering of modal curvatures for damage identification in beams, Procedia Eng. 199 (2017) 1876–1881.
[34] K.-Y. Koo, S.H. Sung, J.W. Park, H.J. Jung, Damage detection of shear buildings using deflections obtained by modal flexibility, Smart Mater. Struct. 19 (11) (2010).

[35] G. Bernagozzi, S. Mukhopadhyay, R. Betti, L. Landi, P.P. Diotallevi, Output-only damage detection in buildings using proportional modal flexibility-based deflections in unknown mass scenarios, Eng. Struct. 167 (2010) 549–566.
[36] C. Rinaldi, J. Ciambella, M. Moroni, V. Gattulli, Optical flow dynamic measurements with high-speed camera on a small-scale steel frame structure, in: A. Carcaterra, A. Paolone, G. G. (Eds.), Proceedings of XXIV AIMETA Conference 2019. AIMETA 2019, in: Lecture Notes in Mechanical Engineering, 2020, pp. 1543–1555.
[37] D. Foti, V. Gattulli, F. Potenza, Output-only identification and model updating by dynamic testing in unfavorable conditions of a seismically damaged building, Comput.-Aided Civ. Infrastruct. Eng. 29 (9) (2014) 659–675.
[38] E. Antonacci, A. DeStefano, V. Gattulli, M. Lepidi, E. Matta, Comparative study of vibration-based parametric identification techniques for a three-dimensional frame structure, J. Struct. Control Health Monit. 19 (5) (2012) 579–608.
[39] R. Brincker, L. Zhang, P. Andersen, Modal identification of output-only systems using frequency domain decomposition, Smart Mater. Struct. 10 (2001) 441–445.
[40] B. Peeters, G.D. Roeck, Stochastic system identification for operational modal analysis: a review, J. Dyn. Syst. Meas. Control 123 (4) (2001) 659–667.
[41] M. Döhler, F. Hille, L. Mevel, W. Rücker, Structural health monitoring with statistical methods during progressive damage test of S101 bridge, Eng. Struct. 69 (2014) 183–193.
[42] J. Ciambella, F. Vestroni, The use of modal curvatures for damage localization in beam-type structures, J. Sound Vib. 340 (2015) 126–137.
[43] J. Ciambella, A. Pau, F. Vestroni, Modal curvature-based damage localization in weakly damaged continuous beams, Mech. Syst. Signal Process. 121 (2019) 171–182.